Development of a multi-layer microfluidic array chip to culture and replate uniform-sized embryoid bodies without manual cell retrieval†

Edward Kang,‡[a] Yoon Young Choi,‡[a] Yesl Jun,[a] Bong Geun Chung*[b] and Sang-Hoon Lee*[a]

Received 7th May 2010, Accepted 14th July 2010
DOI: 10.1039/c0lc00005a

We have developed a multi-layer, microfluidic array platform containing concave microwells and flat cell culture chambers to culture embryonic stem (ES) cells and regulate uniform-sized embryoid body (EB) formation. The main advantage of this platform was that EBs cultured within the concave microwells of a bottom layer were automatically replated into flat cell culture chambers of a top layer, following inversion of the multi-layer microfluidic array platform. This allowed EB formation and EB replating to be controlled simultaneously inside a single microfluidic device without pipette-based manual cell retrieval, a drawback of previous EB culture methods.

Embryonic stem (ES) cells can self-renew and differentiate into various cell types.[1] Due to their potential of unlimited pluripotency and differentiation, ES cells are of great interest in regenerative medicine and cell-based therapies.[2,3] In general, ES cells spontaneously form cell aggregates, called embryoid bodies (EBs), which consist of three germ layers. Various microengineering approaches have been developed to generate and control EBs *in vitro*.[4–12] For example, polymeric microwell arrays have been used to generate EBs in a homogeneous manner.[4–6,13] The EBs could be harvested and subsequently replated onto matrigel substrates to investigate EB size-dependent ES cell-derived endothelial cell differentiation.[6] One drawback of these PEG microwell array systems, however, is the requirement for manual manipulations using a pipette to harvest and replate the EBs prior to inducing further EB differentiation. The bio flip chip has also been developed to pattern mouse ES cells onto cell culture dishes.[14] The bio flip chip enabled the control of cell-cell contact and colony formation of ES cells, showing that cell-cell interaction decreased the efficiency of colony formation. Although the effect of cell-cell interaction on colony formation of the ES cells was investigated in a bio flip chip, this system requires spacer gasket and binder clips for the chip assembling and flipping process. Alternatively, EBs can be generated by using a membrane-based microfluidic device.[7] Although these microfluidic platforms hold great potential in the control of EBs, they cannot harvest EBs. Furthermore, we have developed a poly(dimethylsiloxane) (PDMS)-based concave microwell array system for the generation of controlled-sized EBs.[15] Concave microwells, similar to the contour of EBs, generated homogeneous EBs, resulting in EB size-mediated neuronal differentiation. Quantitative analysis showed that the neurite numbers and average lengths of larger EBs were much higher than those of smaller EBs. However, this approach also required pipettes to harvest the EBs and replate them onto laminin substrates.

To address the limitations of a pipette-based manual cell-retrieval process associated with previous microengineering methods, we have developed a 3 × 3 multi-layer PDMS microfluidic array platform, consisting of concave microwells (bottom layer) for the formation of uniform-sized EBs and flat cell culture chambers (top layer) for replating the EBs (Fig. 1, see supplementary data for detailed materials and methods†). Cells were seeded into microfluidic channels using a syringe pump and were docked within concave microwells

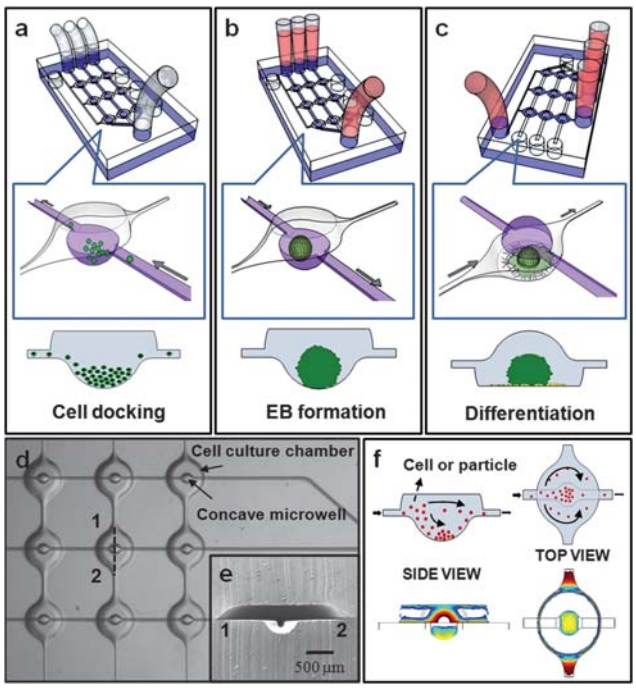

Fig. 1 A 3 × 3 multi-layer microfluidic device containing concave microwells and flat cell-culture chambers. (a) Schematic of the cell docking within concave microwells at the bottom layer. (b) Schematic of the EB formation within microwells in a medium perfusion multi-layer microfluidic device. (c) EBs on flat cell-culture chambers after inversion of the microfluidic device, resulting in the retrieval of EBs from the concave microwells. (d) SEM image of the 3 × 3 multi-layer microfluidic device. (e) Cross-sectional image (1–2 line) of the concave microwells and cell culture chambers. (f) Schematic of the movement of cells within the concave microwells at suitable velocity (top) and simulated results of uniform shear stress on the surface of concave microwells (bottom).

[a]*Department of Biomedical Engineering, Korea University, Seoul, Korea. E-mail: dbiomed@korea.ac.kr*
[b]*Department of Bionano Engineering, Hanyang University, Ansan, Korea. E-mail: bchung@hanyang.ac.kr*

† Electronic supplementary information (ESI) available: Materials and methods; Table: PDMS surface conditions used to generate EBs and induce neural progenitor cell and neuronal differentiation; Figure: cell docking behavior within cylindrical microwells. See DOI: 10.1039/c0lc00005a

‡ These authors contributed equally to this work.

(500 μm in width and 150–250 μm in depth) in a bottom layer, resulting in the formation of homogeneously sized EBs (Fig. 1a–b), because the shape of concave microwells was similar to EBs as we have previously described.[15] The microfluidic device was inverted to harvest EBs from concave microwells and the harvested EBs were spontaneously replated into flat cell culture chambers (2 mm in width and 500 μm in depth) by gravity (Fig. 1c). This platform did not require any pipette-based manual cell retrieval and the EBs were replated into flat cell culture chambers without any of the physical and mechanical manipulations required by previous approaches. The medium was orthogonally perfused into the flat cell culture chambers using an osmotic pump[16] to induce neural progenitor cell and neuronal differentiation. Fig. 1d shows a phase contrast image of a 3 × 3 multi-layer microfluidic array and Fig. 1e shows a cross-sectional scanning electron microscope (FE-SEM, JEOL 4701F, JAPAN) image of a concave microwell and flat cell culture chamber. Computational fluidic dynamic (CFD) simulation also showed the uniform shear stress on the surface of the concave microwells (Fig. 1f, bottom). The PDMS surface conditions were optimized to generate uniform EBs within the concave microwells by various surface treatments, such as poly-L-lysine (PLL) with laminin, PLL with laminin and oxygen plasma treatment (Supplementary Table 1†).

Uniform cell docking within the concave microwells of a multi-layer microfluidic device was important in forming homogeneous EBs. We hypothesized that this uniform cell docking could be controlled by adjusting fluid flow rates and the concave microwell may have better cell docking capability than a cylindrical one. We, therefore, optimized the syringe pump-based flow rate conditions and confirmed these optimized flow rates by CFD analysis (Fig. 2). We observed that, at a lower flow rate (0.02 mL h^{-1}), almost 50% of the cells were docked within deeper concave microwells (500 μm in width, 250 μm in depth) near the inlet (well numbers 1, 4, and 7 in Fig. 2a). A higher flow rate (0.1 mL h^{-1}), however, allowed for uniform cell docking of 8–12 cells per well within deeper concave microwells. This difference may have been due to velocity streamline patterns, in that lower flow rates resulted in shallower streamline patterns within the concave microwells.[17,18] The cells are more easily exposed to velocity streamline profiles at a higher flow rate, allowing for uniform cell docking within concave microwells. We also observed cell docking in shallower microwells (500 μm in width, 150 μm in depth) (Fig. 2b). Interestingly, fewer cells were docked in the shallower microwells than in the deeper microwells, regardless of flow rates, due to the greater penetration into shallower microwells. As a result, the combination of faster flow speed and shear-protective deeper microwells resulted in a higher cell docking efficiency and more uniform numbers of cells in a multi-layer microfluidic array platform. Fig. 2c–d shows the microparticle-based computer simulation of cell number analysis. For the simulation analysis, we used microparticles of the same size and density as the cells. The numbers of cells docking within deeper (Fig. 2c) and shallower (Fig. 2d) microwells increased with decreasing flow rate, whereas the numbers of cells were more uniform at a fast flow speed, showing that simulation analysis closely corresponded to the experimental data.

To test our hypothesis that the shape of microwells would enable the control of cell docking efficiency and uniform cell docking, we analyzed cell docking within cylindrical microwells (Supplementary

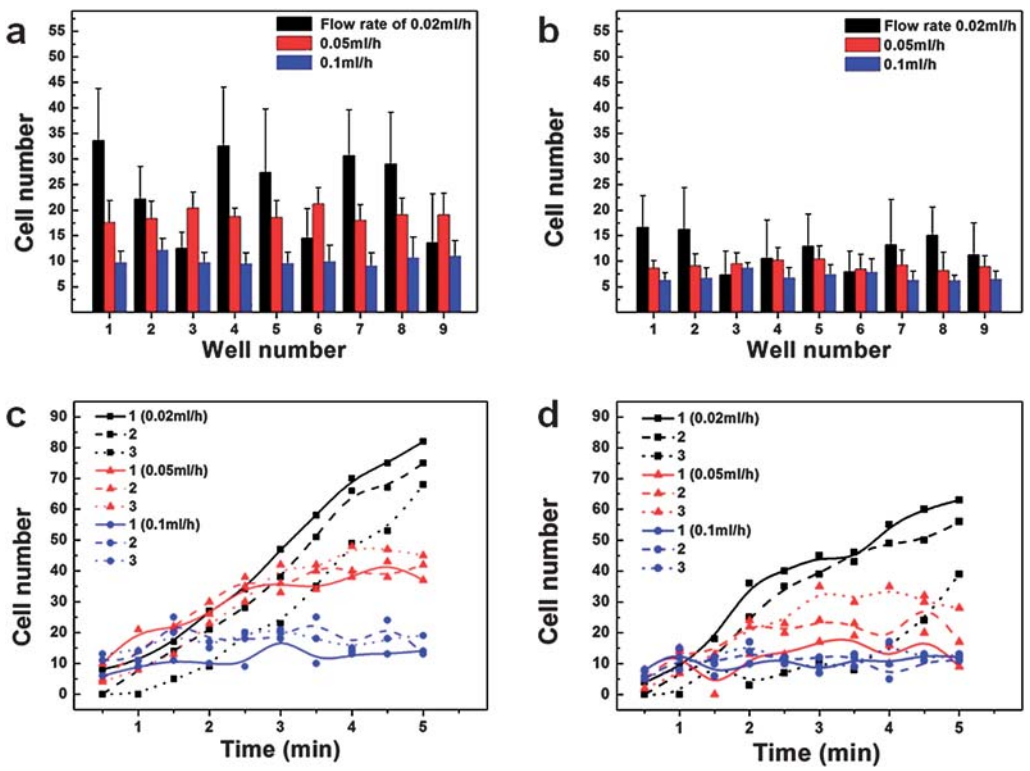

Fig. 2 Cell docking within concave microwells. (a,b) Numbers of cells docked within (a) deeper microwells (500 μm width, 250 μm depth) and (b) shallower microwells (500 μm width, 150 μm depth). Microwells located close to the inlet were designated 1, 4, and 7, and microwells near the outlet were designated 3, 6, and 9 (N = 10). (c,d) Computer simulation-based analysis of numbers of cells within (c) deeper and (d) shallower microwells. The microwell near the inlet was designated 1 and the microwell near the outlet was designated 3.

Figure 1†). In these cylindrical microwells, most cells were docked on the edge, because of non-uniform shear stress and lower velocity penetration. Interestingly, the number of cells docked within cylindrical microwells increased with increasing flow rate, resulting in non-uniform cell docking (Supplementary Figure 1a-b†). In cylindrical microwells near the inlet, most cells were easily trapped and accumulated on the edge (well numbers 1, 4, and 7). In contrast, the number of cells docked within concave microwells decreased with increasing flow rate, resulting in uniform cell docking, because the pattern of the velocity streamline was similar to the hemispherical shape of these microwells, showing that the cells were easily removed by fast flow speed. Therefore, we demonstrated that concave microwells enabled the control of more uniform cell docking as compared to cylindrical microwells.

After optimizing the flow rates and concave microwell depths for uniform cell docking, we studied EB-derived differentiation in the multi-layer microfluidic device. We observed the formation of homogeneous EBs within the concave microwells, indicating that the cells were uniformly docked (Fig. 3a), with EB diameters increasing over time to 250–450 μm (Fig. 3b). Using live/dead assays, we found that most cells cultured within these microwells for 3 days remained viable after replating into flat cell culture chambers (Fig. 3c), showing that the inversion of the multi-layer microfluidic platform for replating EBs did not damage the cells. Furthermore, as a proof-of-concept, we assessed EB-derived neural progenitor cells and neuronal differentiation in the multi-layer microfluidic device (Fig. 3d). To induce neural progenitor cells and neuronal differentiation, we inverted a multi-layer microfluidic device to detach EBs from microwells and automatically replate them into cell culture chambers pretreated with PLL and laminin, which resulted in greater EB-derived neural progenitor cells and neuronal differentiation than observed in untreated culture chambers (Supplementary Table 1†). We found that EB-derived neural progenitor cells and neurons formed a single cell monolayer in flat cell culture chambers. Although we were able to generate and replate EBs in a single microfluidic device and induce neural progenitor cells and neuronal differentiation, some limitations remained, such as the inability to minimize the background fluorescence of immunostained images, because PDMS channels may adsorb the antibody or staining solution more than coverslips or well-plate substrates.

In summary, the main advantage of this system was that we could generate homogeneous EBs within concave microwells in a controlled manner and automatically replate EBs into flat cell culture chambers inside a single microfluidic device without the need for any pipette-based manual cell retrieval. The numbers of the cells docking inside microwells were homogeneously controlled by applying fluidic flow rates and the effect of the shear stress on ES cell proliferation and differentiation could be investigated. Multi-layer microfluidic array platforms may, therefore, be a potentially powerful approach for studying EB-derived ES cell differentiation. Furthermore, by integrating on-chip valve systems into a microfluidic device to precisely control individually addressable soluble factors, these platforms could be used to control cell behavior in a high-throughput manner. Integrated multi-layer microfluidic array platforms with on-chip valve systems may be used to deliver soluble factors into each microwell and perform high-throughput drug screening, making these platforms a powerful tool for directing stem cell fate and controlling cell-soluble factor interaction in a well-defined microenvironment.

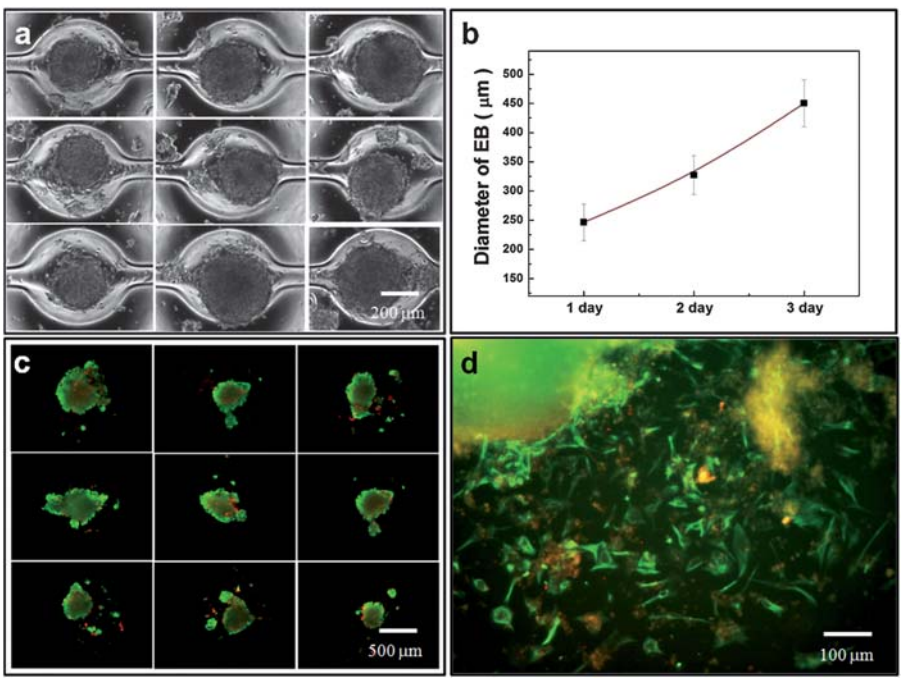

Fig. 3 EB formation and differentiation in a multi-layer microfluidic device. (a) Homogeneous EB formation within concave microwells (500 μm width, 250 μm depth). Scale bar represents 200 μm. (b) Analysis of EB diameters in a multi-layer microfluidic device. (c) Cell viability of EBs cultured within concave microwells for 4 days (green, live cells; red, dead cells). (d) EB-derived neural progenitor cell and neuronal differentiation. Neural progenitor cells and neurons cultured on flat cell culture chambers for an additional 8 days were immunostained with antibodies to nestin (green) and neurofilament (red).

Acknowledgements

This study was supported by a grant from the NRL (National Research Lab) program, the Korea Science and Engineering Foundation (KOSEF), Republic of Korea (No. R0A-2007-000-20086-0) and the Conversing Research Center Program through the National Research Foundation of Korea (NRF) funded by the Ministry of Education, Science and Technology (No. 2009-0082201).

References

1 B. Bhattacharya, S. Puri and R. K. Puri, *Curr. Stem Cell Res. Ther.*, 2009, **4**, 98–106.
2 P. Taupin, *J. Neural Eng.*, 2007, **4**, R59–63.
3 A. M. Wobus and K. R. Boheler, *Physiol. Rev.*, 2005, **85**, 635–678.
4 H. C. Moeller, M. K. Mian, S. Shrivastava, B. G. Chung and A. Khademhosseini, *Biomaterials*, 2008, **29**, 752–763.
5 J. M. Karp, J. Yeh, G. Eng, J. Fukuda, J. Blumling, K. Y. Suh, J. Cheng, A. Mahdavi, J. Borenstein, R. Langer and A. Khademhosseini, *Lab Chip*, 2007, **7**, 786–794.
6 Y. S. Hwang, B. G. Chung, D. Ortmann, N. Hattori, H. C. Moeller and A. Khademhosseini, *Proc. Natl. Acad. Sci. U. S. A.*, 2009, **106**, 16978–16983.
7 Y. S. Torisawa, B. H. Chueh, D. Huh, P. Ramamurthy, T. M. Roth, K. F. Barald and S. Takayama, *Lab Chip*, 2007, **7**, 770–776.
8 R. Peerani, B. M. Rao, C. Bauwens, T. Yin, G. A. Wood, A. Nagy, E. Kumacheva and P. W. Zandstra, *EMBO J.*, 2007, **26**, 4744–4755.
9 J. Park, C. H. Cho, N. Parashurama, Y. Li, F. Berthiaume, M. Toner, A. W. Tilles and M. L. Yarmush, *Lab Chip*, 2007, **7**, 1018–1028.
10 L. H. Lee, R. Peerani, M. Ungrin, C. Joshi, E. Kumacheva and P. Zandstra, *Stem Cell Res.*, 2009, **2**, 155–162.
11 R. Peerani, K. Onishi, A. Mahdavi, E. Kumacheva and P. W. Zandstra, *PLoS One*, 2009, **4**, e6438.
12 C. L. Bauwens, R. Peerani, S. Niebruegge, K. A. Woodhouse, E. Kumacheva, M. Husain and P. W. Zandstra, *Stem Cells*, 2008, **26**, 2300–2310.
13 J. C. Mohr, J. Zhang, S. M. Azarin, A. G. Soerens, J. J. de Pablo, J. A. Thomson, G. E. Lyons, S. P. Palecek and T. J. Kamp, *Biomaterials*, 2010, **31**, 1885–1893.
14 A. Rosenthal, A. Macdonald and J. Voldman, *Biomaterials*, 2007, **28**, 3208–3216.
15 Y. Y. Choi, B. G. Chung, D. H. Lee, A. Khademhosseini, J. H. Kim and S. H. Lee, *Biomaterials*, 2010, **31**, 4296–4303.
16 J. Y. Park, C. M. Hwang and S. H. Lee, *Lab Chip*, 2007, **7**, 1673–1680.
17 A. Manbachi, S. Shrivastava, M. Cioffi, B. G. Chung, M. Moretti, U. Demirci, M. Yliperttula and A. Khademhosseini, *Lab Chip*, 2008, **8**, 747–754.
18 M. Khabiry, B. G. Chung, M. J. Hancock, H. C. Soundararajan, Y. Du, D. Cropek, W. G. Lee and A. Khademhosseini, *Small*, 2009, **5**, 1186–1194.

